



CHORUS

This is the accepted manuscript made available via CHORUS. The article has been published as:

BCS-BEC Crossover and Topological Phase Transition in 3D Spin-Orbit Coupled Degenerate Fermi Gases

Ming Gong, Sumanta Tewari, and Chuanwei Zhang

Phys. Rev. Lett. **107**, 195303 — Published 4 November 2011

DOI: [10.1103/PhysRevLett.107.195303](https://doi.org/10.1103/PhysRevLett.107.195303)

BCS-BEC Crossover and Topological Phase Transition in 3D Spin-Orbit Coupled Degenerate Fermi Gases

Ming Gong¹, Sumanta Tewari², and Chuanwei Zhang^{1*}

¹*Department of Physics and Astronomy, Washington State University, Pullman, WA, 99164 USA*

²*Department of Physics and Astronomy, Clemson University, Clemson, SC 29634 USA*

We investigate the BCS-BEC crossover in three dimensional degenerate Fermi gases in the presence of spin-orbit coupling (SOC) and Zeeman field. We show that the superfluid order parameter destroyed by a large Zeeman field can be restored by the SOC. With increasing strengths of the Zeeman field, there is a series of topological quantum phase transitions from a non-topological superfluid state with fully gapped fermionic spectrum to a topological superfluid state with four topologically protected Fermi points (*i.e.*, nodes in the quasiparticle excitation gap) and then to a second topological superfluid state with only two topologically protected Fermi points. We show that the topological phase transitions can be probed using the experimentally realized momentum resolved photoemission spectroscopy.

PACS numbers: 03.75Ss, 74.20.-z, 03.75.Lm

Ultra-cold Fermi gases with tunable atom interaction through Feshbach resonance [1] have garnered tremendous attention recently [2] for their potential use as an ideal platform for emulating many important physical phenomena. Interesting physics, including the crossover from Bardeen-Cooper-Schrieffer (BCS) superfluid to Bose-Einstein condensate (BEC) of molecules [3], universal properties in the unitary limit [4], vortices [5], *etc.*, have been observed in experiments. In addition to single species Fermi atoms with equal population in two spin states, Fermi gases with population and mass imbalance have also been intensively studied [6–8]. Here the population imbalance between two pseudo-spin states serves as an effective Zeeman field, which have stimulated enormous experimental efforts on searching for the Fulde-Ferrel-Larkin-Ovchinnikov state in Fermi gases [9].

The pseudospin of atoms can couple with not only the effective Zeeman field, but also with the orbital degrees of freedom of atoms (*i.e.*, spin-orbit coupling (SOC)). The recent experimental realization of SOC for ultra-cold atoms [10] opens a completely new avenue for investigating the SOC physics using degenerate cold Fermi gases. In this context, it is natural to investigate the BCS-BEC crossover physics [11, 12] in the presence of SOC, which is an important and interesting problem by itself and has not been investigated previously. Furthermore, such crossover physics is also important because the *s*-wave superfluid, together with SOC and Zeeman field, may yield intriguing chiral *p*-wave physics [13] such as Majorana fermions with non-Abelian statistical properties [14]. However, such chiral *p*-wave physics may be observable only in the crossover region where the superfluid order parameter is large and thus robust against finite temperature effects.

In this Letter, we investigate the BCS-BEC crossover and the topological properties of a three-dimensional (3D) uniform *s*-wave superfluid in the presence of both Zeeman field and Rashba-type of SOC. Under the mean

field approximation, we derive the superfluid gap and atom density equations and solve them self-consistently in the BCS-BEC crossover region. Our main results are:

(I) It is well known that the superfluid can be destroyed by the Zeeman field beyond a critical value for a given *s*-wave interaction strength [15]. We show that a finite SOC strength can restore the superfluid pair potential back to the system even when the Zeeman field is well above the critical value.

(II) At zero temperature, the nonzero superfluid pair potential in the presence of SOC supports, with increasing strength of the Zeeman field, a series of 3D topological quantum phase transitions [16] from a non-topological superfluid state with fully gapped fermionic excitations to a topological superfluid state with four protected Fermi points (*i.e.*, gap nodes) and then to a second topological superfluid state with only two protected Fermi points (see Fig. 3). Such 3D topological superfluids are gapless without Majorana fermions because of the existence of Fermi points, as opposed to the 2D fully gapped topological superfluids with Majorana fermions [14].

(III) The superfluid phases separated by the topological quantum critical points are indistinguishable in terms of the superfluid pair potential, which remains continuous across both transitions. On the other hand, the superfluid phases are distinguishable in terms of the ground states which have very different excitation spectra. The non-topological superfluid state is a usual fully gapped *s*-wave superfluid, while the topological superfluid states are gapless even if the superfluid pair potentials are still strictly *s*-wave! These peculiar gapless topological superfluids are new phases of matter and here we show how to identify such phases and the corresponding quantum critical points using the experimentally already realized momentum-resolved photoemission spectroscopy [17, 18].

Mean-field theory: The system we consider is a 3D uniform *s*-wave fermionic superfluid with the atom density *n* and which is subject to Rashba SOC in the *xy* plane

and a Zeeman field along the z direction. The dynamics of the Fermi gas can be described by the Hamiltonian $H = H_0 + H_{\text{int}}$, where the single particle Hamiltonian $H_0 = \sum_{\mathbf{k}\gamma\gamma'} c_{\mathbf{k}\gamma}^\dagger [\xi_{\mathbf{k}} I + \alpha(k_y \sigma_x - k_x \sigma_y) + \Gamma \sigma_z]_{\gamma\gamma'} c_{\mathbf{k}\gamma'}$, $\gamma = \uparrow, \downarrow$ are the pseudo-spin of the atoms, $\xi_{\mathbf{k}} = \epsilon_{\mathbf{k}} - \mu$, $\epsilon_{\mathbf{k}} = \hbar^2 k^2 / 2m$ is the free particle energy, μ is the chemical potential, α is the Rashba SOC strength, I is the 2×2 unit matrix, σ_i is the Pauli matrix, Γ is the strength of the Zeeman field, and $c_{\mathbf{k}\gamma}$ is the atom annihilation operator. $H_{\text{int}} = g \sum_{\mathbf{k}} c_{\mathbf{k}\uparrow}^\dagger c_{-\mathbf{k}\downarrow}^\dagger c_{-\mathbf{k}\downarrow} c_{\mathbf{k}\uparrow}$ is the s -wave scattering interaction with $g = 4\pi \hbar^2 \bar{a}_s / m$, and the scattering length \bar{a}_s can be tuned by the Feshbach resonance [1].

In the mean-field approximation, the s -wave superfluid pair potential $\Delta = g \sum_{\mathbf{k}} \langle c_{\mathbf{k}\downarrow} c_{-\mathbf{k}\uparrow} \rangle$ and $H_{\text{int}} = -\Delta^2 / g + \Delta \sum_{\mathbf{k}} (c_{\mathbf{k}\downarrow} c_{-\mathbf{k}\uparrow} + c_{-\mathbf{k}\uparrow}^\dagger c_{\mathbf{k}\downarrow}^\dagger)$. Under the Nambu spinor basis $\Psi_{\mathbf{k}} = (c_{\mathbf{k}\uparrow}, c_{\mathbf{k}\downarrow}, c_{-\mathbf{k}\downarrow}^\dagger, -c_{-\mathbf{k}\uparrow}^\dagger)^T$, the Hamiltonian is $H = \frac{1}{2} \sum_{\mathbf{k}} \Psi_{\mathbf{k}}^\dagger M_{\mathbf{k}} \Psi_{\mathbf{k}} - \Delta^2 / g + \sum_{\mathbf{k}} \xi_{\mathbf{k}}$, where

$$M_{\mathbf{k}} = \begin{pmatrix} H_0(\mathbf{k}) & \Delta I \\ \Delta I & -\sigma_y H_0^*(-\mathbf{k}) \sigma_y \end{pmatrix} \quad (1)$$

preserves the particle-hole symmetry. The quasiparticle excitation energy

$$E_{\mathbf{k}\pm}^\lambda = \lambda \sqrt{\xi_{\mathbf{k}}^2 + \alpha^2 k_\perp^2 + \Gamma^2 + |\Delta|^2 \pm 2E_0} \quad (2)$$

is the eigenvalue of $M_{\mathbf{k}}$, where $\lambda = \pm$ correspond to the particle and hole branches, $E_0 = \sqrt{\Gamma^2 (\xi_{\mathbf{k}}^2 + |\Delta|^2) + \alpha^2 k_\perp^2 \xi_{\mathbf{k}}^2}$, and $k_\perp = \sqrt{k_x^2 + k_y^2}$. For $\alpha = \Gamma = 0$, Eq. (2) reduces to $E_{\mathbf{k}}^\lambda = \lambda \sqrt{\xi_{\mathbf{k}}^2 + |\Delta|^2}$ in the standard BCS theory.

Diagonalizing the total Hamiltonian using the Bogoliubov transformation and following the standard procedure [2], we obtain the gap equation

$$\frac{m\Delta}{4\pi \hbar^2 a_s} = -\Delta \sum_{\mathbf{k}, \eta} (1 - \eta \Gamma^2 / E_0) f(E_{\mathbf{k}, \eta}^+) - \frac{1}{2\epsilon_{\mathbf{k}}}, \quad (3)$$

where $f(E_{\mathbf{k}, \eta}^+) = \tanh(\beta E_{\mathbf{k}, \eta}^+ / 2) / 4E_{\mathbf{k}, \eta}^+$, $\beta = 1/k_B T$, T is the temperature, and k_B is the Boltzmann constant. Following the standard procedure [2], the ultra-violet divergence at the large \mathbf{k} in Eq. (3) has been regularized through subtracting the term $1/2\epsilon_{\mathbf{k}}$ and a_s is defined as the renormalized scattering length. The total number of atoms can be obtained using a similar method [2]

$$N = 2 \sum_{\mathbf{k}, \eta} \left[\frac{\eta(\alpha^2 k_\perp^2 + \Gamma^2)}{E_0} - 1 \right] \xi_{\mathbf{k}} f(E_{\mathbf{k}, \eta}^+) + \frac{1}{2}. \quad (4)$$

We self-consistently solve the gap equation (3) and the number equation (4) for different parameters $(\alpha K_F, \Gamma, \nu, T)$ for a fixed atom density n to determine Δ and μ . Here $\nu = 1/K_F a_s$ and $K_F = (3\pi^2 n)^{1/3}$ is the Fermi vector for a non-interacting Fermi gas with the same density at $\Gamma = \alpha = 0$. The energy unit is chosen as the Fermi energy $E_F = \hbar^2 K_F^2 / 2m$.

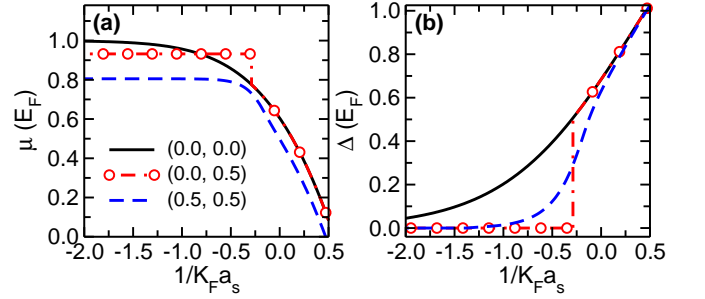


FIG. 1. (Color online) Plot of μ (a) and Δ (b) versus $\nu = 1/K_F a_s$ for different parameters $(\alpha K_F, \Gamma)$ at $T = 0$.

BCS-BEC crossover: Without SOC, it is well-known that the Zeeman field Γ can lift the spin degeneracy between \uparrow and \downarrow , thus destroys the Cooper pairing when the Zeeman field is larger than the pairing interaction energy [15]. This result can also be understood from Eq. (2), where the quasiparticle excitation gap $E_g = \min_{\mathbf{k}} \left| \sqrt{\xi_{\mathbf{k}}^2 + |\Delta|^2} - \Gamma \right| = 0$ for a suitable chosen \mathbf{k} when $\alpha = 0$ and $|\Gamma| > \Delta$. With SOC, the single particle Hamiltonian H_0 has two bands and each band contains both spin \uparrow and \downarrow components even with a large Zeeman field, leading to nonzero superfluid Cooper pairing between two fermions in the same band with opposite momenta.

Such SOC induced nonzero superfluid pair potential can be clearly seen in Fig. 1, where we plot the change of μ and Δ with respect to $\nu = 1/K_F a_s$ for different parameters $(\alpha K_F, \Gamma)$ at $T = 0$. In the BEC side, the SOC strength αK_F and the Zeeman field Γ do not have significant influence on Δ because all fermion atoms form bound molecules. Hence we mainly focus on the BCS side. At $\alpha = 0$, the superfluid pair potential is destroyed when $\Gamma > \Delta$, as expected. In contrast, Δ and μ are independent of Γ when $\Gamma < \Delta$. This can be understood from the fact that, without SOC, Eq. (3) and (4) are independent of Γ when $\Gamma < \Delta$. Therefore there is a sudden jump of μ and Δ at $\Gamma = \Delta$ for $\alpha = 0$, as clearly seen from Fig. 1. We see Δ can be restored to non-zero values even for a large Γ when αK_F is switched on.

In Fig. 2a, we plot Δ with respect to αK_F on the

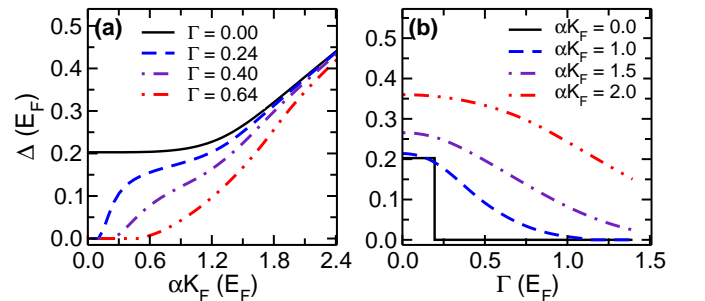


FIG. 2. (a) Plot of Δ with respect to αK_F for different Γ . (b) Plot of Δ with respect to Γ for different αK_F . $\nu = -1$, $T = 0$.

BCS side with $\nu = -1$ and $T = 0$. For other values of ν and T , the results are similar. When $\Gamma < \Delta$, the pair potential Δ approaches the same point (determined by the interaction strength ν) for different Γ when $\alpha \rightarrow 0$. Δ vanishes for Γ beyond a critical value at $\alpha = 0$, but can be restored when α is nonzero. Therefore the superfluid order can still be observed even with a large Zeeman field. In Fig. 2b, we plot Δ versus Γ for different SOC. Without SOC, we observe a sudden jump of the pair potential at $\Gamma = \Delta$, as expected. With non-zero SOC, Δ decreases smoothly with Γ . At large Γ , the numerical results can be fitted with $\Delta \sim \chi\Gamma^{-2}$ with the constant χ depending on the SOC.

Topological phase transition: The existence of nonzero superfluid pair potentials induced by the SOC does not automatically determine the topological properties of the superfluid. In a 3D uniform superfluid, the momentum is a good quantum number and the topological order of the superfluid can be classified by the number of Fermi points [16] (*i.e.*, the nodes such that $E_{\mathbf{k},-}^+ = 0$) in the quasiparticle excitation spectrum for fixed external parameters $(\alpha K_F, \Gamma, \nu)$ and at $T = 0$. From Eq. (2), we see $E_{\mathbf{k},-}^+ E_{\mathbf{k},+}^+ = (\xi_{\mathbf{k}}^2 - \Gamma^2 + \Delta^2 - \alpha^2 k_{\perp}^2)^2 + 4\Delta^2 \alpha^2 k_{\perp}^2$, therefore there is always a finite gap for $k_{\perp} > 0$ and all Fermi points must lie along k_z axis, see Fig. 3a. At $k_{\perp} = 0$, the quasiparticle excitation gap becomes

$$E_g = |\Gamma - \sqrt{\bar{\mu}^2 + \Delta^2}|, \quad (5)$$

where $\bar{\mu} = \mu - \hbar^2 k_z^2 / 2m$.

We choose $\alpha K_F = E_F$, $\nu = -0.1$, $T = 0$, and study the topological phase transition driven by the varying Γ . In Fig. 3b, we plot $E_g = 0$ in the (k_z, Γ) plane and count the number of Fermi points for a fixed Γ . There are three different phases: (A) a fully gapped non-topological superfluid state without Fermi points when $\Gamma < \Delta$, (B) a superfluid state with four Fermi points for each Γ when $\Delta < \Gamma < \Gamma_c = \sqrt{\mu^2 + \Delta^2}$ and (C) a second superfluid state with two Fermi points for each Γ when $\Gamma > \Gamma_c$. Around each Fermi point, we have checked that the quasiparticle energy dispersion $E_{\mathbf{k},-}^{\lambda}$ is linear, therefore the Fermi point behaves like a Dirac point, and is topologically protected with a topological charge $N_a = \pm 1$. Here N_a is defined by the 3D topological invariant $N_a = \frac{1}{24\pi^2} \epsilon_{\mu\nu\xi\lambda} \text{tr} \oint_{\Sigma_a} dS^{\lambda} G \frac{\partial G^{-1}}{\partial k_{\mu}} G \frac{\partial G^{-1}}{\partial k_{\nu}} G \frac{\partial G^{-1}}{\partial k_{\xi}}$ [16], where $G^{-1} = ik_0 - M_{\mathbf{k}}$ is the Green function for the quasiparticle excitation, Σ_a is a 3D surface around the isolated Fermi point $(0, \mathbf{k}_a)$, k_0 is the energy, and "tr" stands for the trace over the relevant spin indices. At each of the two critical points as a function of Γ ($\Gamma = \Delta$ and $\Gamma = \sqrt{\mu^2 + \Delta^2}$), Fermi points with opposite topological charges merge and form a topologically trivial Fermi point with $N_a = 0$, which then disappear with the Zeeman field. Note that topologically protected Fermi points with $N_a = \pm 1$ in phases B and C are protected in the sense that they cannot disappear with Γ

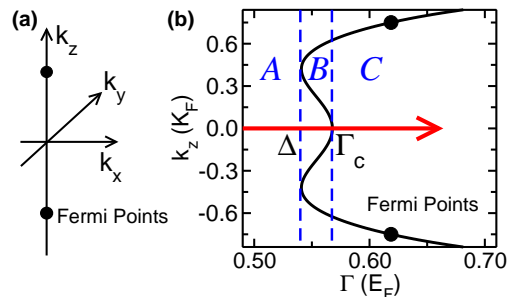


FIG. 3. (a) Fermi points along the k_z axis. (b) Quantum phase transition in a 3D uniform superfluid driven by the Zeeman field at $T = 0$, $\alpha K_F = E_F$, and $\nu = -0.1$. The solid line represents $E_g = 0$. The change of E_g along the red arrow is shown in Fig. 4a.

except at quantum critical points (where they pair-wise merge to become topologically trivial and disappear with the Zeeman field [16]). Such a series of two topological quantum phase transitions (two quantum critical points) is quite different from the situation encountered across a p -wave Feshbach resonance (*i.e.*, driven by varying the interaction strength), where a 3D gapless $p_x + ip_y$ BCS superfluid becomes a gapped BEC at a single topological critical point at $\mu = 0$ [19]. In addition, the superfluid pair potential is still finite in our system, while it vanishes in the $p_x + ip_y$ superfluid [19] when the quasiparticle excitation gap closes.

Observation of topological phase transition: The peculiar phases B and C with strictly s -wave pair potentials, but topologically protected Fermi points, are new phases of matter. Here we show how to identify such phases and the corresponding topological quantum critical points by the momentum resolved photoemission spectroscopy [17, 18]. Note that topological quantum critical points are not easily observable in usual experimental probes because of the absence of broken symmetries and emergent order parameters at such transitions. In the photoemission experiments, $E_{\mathbf{k},-}^+$ for a fixed (or a small range of) k_z can be measured by analyzing the part of the time of flight image with the same k_z . This measurement yields E_g as a function of k_z and Γ , from which the phase diagram in Fig. 3b can be mapped out through $E_g(k_z, \Gamma) = 0$. In the following, we describe the change of E_g for $k_z = 0$ and increasing Γ (the horizontal red arrow in Fig. 3b). The results are similar for $k_z \neq 0$.

For $k_z = 0$, E_g does not close at the boundary between phases A and B, therefore the quasiparticle excitations are gapped non-topological when $\Gamma < \Gamma_c$ (*i.e.*, A and B phases merge together). E_g vanishes at Γ_c and then reopens when $\Gamma > \Gamma_c$, where the quasiparticle excitations become topologically non-trivial. In Fig. 4a, we plot E_g at $\mathbf{k} = 0$ with respect to Γ at $T = 0$. The corresponding Δ and μ are also plotted. When Γ sweeps through $\Gamma_c = 0.56E_F$, E_g first closes and then reopens, indicating a transition from non-topological quasiparticle excitations

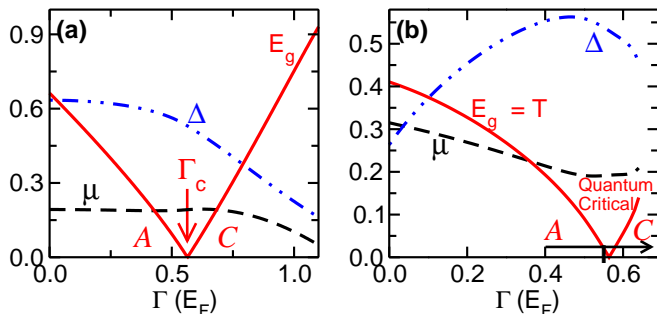


FIG. 4. (a) Plot of E_g , Δ , and μ , with respect to Γ at $\mathbf{k} = 0$. $\nu = -0.1$, $\alpha K_F = E_F$, and $T = 0$. (b) Topological phase crossovers at finite temperature, where the red curve is determined by Eq. 6. The arrow represents the phase crossovers at a fixed temperature. A and C represent regions with gapped non-topological and topological excitations, respectively.

to gapless excitations and then to topological excitations. At Γ_c , we still observe a strong $\Delta = 0.52E_F$, although E_g has a node. For other fixed $k_z \neq 0$, the corresponding Γ_c can also be determined similarly through the vanishing of E_g . Therefore the phase diagram for the 3D topological phase transition in Fig. 3b can be mapped out.

A realistic experiment only works at a finite temperature, which induces thermal excitations and may destroy the superfluid. The percentage of the thermal component in the gas depends strongly on the ratio $E_g/k_B T$. Note that at finite temperature, there is no definite boundary between different phases, *i.e.*, there are only finite temperature phase crossovers. Nevertheless, we still plot the phase lines in Fig. 4b at which

$$E_g(\alpha, \nu, \Gamma, T) = k_B T \quad (6)$$

for the illustration of the topological phase crossover region. Note that E_g also depends on T , and Eq. (6) should be solved self-consistently with Eq. (3) and (4). Therefore the relationship between Δ and Γ here is quite different from the zero temperature case in Fig. 4a. In experiments, the fixed temperature corresponds to a horizontal line (with the arrow) in the phase diagram Fig. 4b. Between phases A and C , there is a quantum critical region where finite temperature generates many quasi-particle excitations.

Experimental parameters: In experiments, the Rashba SOC and Zeeman field can be generated through the coupling between atoms and laser fields [10, 20]. We consider a set of realistic parameters for ^{40}K atom with $n = 5 \times 10^{12} \text{ cm}^{-3}$, corresponding to the Fermi energy $E_F = \hbar \times 3.5 \text{ KHz}$. A large SOC strength $\alpha K_F \sim E_F$ is also attainable [10, 20]. The effective Zeeman field Γ from 0 to E_F can be obtained by tuning the intensity of laser beams [10, 20]. By tuning the s -wave scattering length using the Feshbach resonance [1], we can vary Δ from $\sim 0.1E_F$ to $\sim E_F$. The existence of non-zero superfluid pair potentials induced by the SOC with a large Zeeman field can be detected through the emergence of

vortices [5] in experiments. The topological phase transition can be observed by detecting the change of E_g versus Γ for each fixed k_z using the momentum resolved photoemission spectroscopy [17, 18]. From Fig. 4a, we see for $1/K_F a_s = -0.1$ and $\Gamma = 0.85E_F$, $E_g \sim E_F$, which is much larger than the energy resolution in the photoemission experiment. In experiments, the observed gap E_g first decreases to zero and then increases, which provides a clear signature for the transition from non-topological to topological superfluid phases. Note that the transition temperature T_c from superfluid to normal states in the presence of SOC should be larger than that for the superfluid without SOC [3] because of the enhanced superfluid order parameter Δ (see Fig. 2a) [22]. The temperature needed for the observation of the topological phase crossover in Fig. 4b is clearly lower than T_c , which is nonzero on both sides of the critical Γ_c because of the existence of the non-vanishing Δ .

Summary: In summary, we study the BCS-BEC crossover and the topological phase transitions in 3D uniform spin-orbit coupled degenerate Fermi gases. The predicted SOC induced s -wave superfluid opens new possibilities for generating and observing many new topological phenomena in Fermi gases. The observation of the 3D topological phase transitions using the experimentally already realized photoemission spectroscopy provides a critical first step for searching for non-trivial topological superfluid states (which in 2D support Majorana fermions and the associated non-Abelian statistics [14, 21]) in cold atom s -wave superfluids, which are of not only fundamental but also technological importance.

Note: After we submitted the paper, two manuscripts appeared in arXiv [22, 23], where the BCS-BEC crossover with SOC (but without Zeeman fields) is discussed.

Acknowledgement This work is supported by DARPA-YFA (N66001-10-1-4025), ARO (W911NF-09-1-0248), and DARPA-MTO (FA9550-10-1-0497).

* Corresponding author. Email: cwzhang@wsu.edu

- [1] C. Chin *et al.*, Rev. Mod. Phys. **82**, 1225 (2010).
- [2] S. Giorgini *et al.*, Rev. Mod. Phys. **80**, 1215 (2008).
- [3] C. A. Regal *et al.*, Phys. Rev. Lett. **92**, 040403 (2004); M. W. Zwierlein *et al.*, *ibid.* **92**, 120403 (2004); M. Bartenstein *et al.*, *ibid.* **92**, 120401 (2004).
- [4] J. T. Stewart *et al.*, Phys. Rev. Lett. **104**, 235301 (2010).
- [5] M. W. Zwierlein *et al.*, Nature **435**, 1047 (2005).
- [6] M. W. Zwierlein *et al.*, Science **311**, 492 (2006).
- [7] G. B. Partridge *et al.*, Science **311**, 503 (2006).
- [8] M. Taglieber *et al.*, Phys. Rev. Lett. **100**, 010401 (2008).
- [9] Y. Liao *et al.*, Nature **467**, 567 (2010).
- [10] Y.-J. Lin *et al.*, Nature **471**, 83 (2011).
- [11] M. Holland *et al.*, Phys. Rev. Lett. **87**, 120406 (2001).
- [12] C. A. R. Sá de Melo, Phys. Today **61**, 45 (2008).
- [13] C. Zhang *et al.*, Phys. Rev. Lett. **101**, 160401 (2008).
- [14] C. Nayak *et al.*, Rev. Mod. Phys. **80**, 1083 (2008).

- [15] P. F. Bedaque *et al.*, Phys. Rev. Lett. 91, 247002 (2003).
- [16] G. E. Volovik, *The Universe in a Helium Droplet* (Clarendon Press, Oxford, 2003).
- [17] J. T. Stewart *et al.*, Nature **454**, 744 (2008).
- [18] J. P. Gaebler *et al.*, Nature Phys. **6**, 569 (2010).
- [19] S. S. Botelho and C. A. R. Sa de Melo, J. Low Temp. Phys. 140, 409 (2005); V. Gurarie *et al.*, Phys. Rev. Lett. 94, 230403 (2005).
- [20] J. Ruseckas *et al.*, Phys. Rev. Lett. **95**, 010404 (2005); D. L. Campbell *et al.*, arXiv:1102.3945.
- [21] J. D. Sau *et al.*, Phys. Rev. Lett. **104**, 040502 (2010).
- [22] Z.-Q. Yu and H. Zhai, arXiv:1105.2250.
- [23] H. Hu *et al.*, arXiv:1105.2488.